

# Dusty Sources at the Galactic Center: The $N$ - and $Q$ -band view with VISIR

T. Viehmann<sup>1</sup>

and

A. Eckart<sup>1</sup>

and

R. Schödel<sup>1</sup>

and

J.-U. Pott<sup>1,2</sup>

and

J. Moulaka<sup>1</sup>

## ABSTRACT

We present mid-infrared  $N$ - and  $Q$ -band photometry of the Galactic Center from images obtained with the mid-infrared camera VISIR at the ESO VLT in May 2004. The high resolution and sensitivity possible with VISIR enables us to investigate a total of over 60 point-like sources, an unprecedented number for the Galactic Center at these wavelengths. Combining these data with previous results at shorter wavelengths (Viehmann et al. 2005) enables us to construct SEDs covering the  $H$ - to  $Q$ -band regions of the spectrum, i.e. 1.6 to 19.5  $\mu\text{m}$ . We find that the SEDs of certain types of Galactic Center sources show characteristic features. We can clearly distinguish between luminous Northern Arm bow-shock sources, lower luminosity bow-shock sources, hot stars, and cool stars. This characterization may help clarify the status of presently unclassified sources.

*Subject headings:* Galactic Center — Mid-infrared — Stellar classification

---

<sup>1</sup>I. Physikalisches Institut, Universität zu Köln, Zùlpicher Str. 77, D-50937 Köln, Germany  
[viehmann@ph1.uni-koeln.de](mailto:viehmann@ph1.uni-koeln.de)

<sup>2</sup>ESO, Karl-Schwarzschild-Str. 2, D-85748 Garching, Germany

## 1. Introduction

The Galactic Center is known as a bright source of near- and mid-infrared radiation since the late 1960s (Becklin & Neugebauer 1968, 1969; Low et al. 1969). The main source of near-infrared radiation is photospheric emission from a dense stellar cluster, i.e. a crowded field of point sources, while almost all of the mid-infrared radiation originates from extended gas and dust features as well as dust emission from the circumstellar regions of a dozen individual sources interacting with the more extended Galactic Center interstellar medium.

The nature of the brightest mid-infrared sources is more or less clear – IRS 1W, 2, 5, 10W, and 21 are bow-shock sources, caused by bright stars with strong winds plowing through the ambient gas and dust of the Northern Arm (Tanner et al. 2002, 2003, 2005; Rigaut et al. 2003; Eckart et al. 2004; Geballe et al. 2004). Of the fainter sources, IRS 7 is an M2 supergiant, however, most of the others remain enigmatic.

Combined photometry at near- and mid-infrared wavelengths is an ideal tool to investigate the nature of the bright mid-infrared sources, since it gives information on both the mid-infrared sources themselves and the stellar sources that could be powering them. We therefore present *N*- and *Q*-band photometry of the Galactic Center, obtained with the ESO VLT, in order to further investigate the nature of the mid-infrared sources. Additional data at shorter wavelengths is taken from Viehmann et al. (2005) to provide a more complete picture.

Previous studies at mid-infrared wavelengths have been severely limited in resolution (Becklin et al. 1978  $\sim 2''$ , Gezari et al. 1985  $\gtrsim 1''$ , Stolovy et al. 1996  $\sim 0.7''$ ), however, since the availability of the mid-infrared camera VISIR at the ESO VLT, the Galactic Center can be studied in great detail in the *N*- and *Q*-bands (8-13  $\mu\text{m}$  and 17-24  $\mu\text{m}$ ), with a resolution of 0.3'' to 0.6'' (the diffraction limit of an 8 m telescope), provided that the seeing is good enough. This corresponds to a linear resolution of 2500 to 5000 AU at the distance of 8 kpc to the Galactic Center.

## 2. Observations and data reduction

### 2.1. VISIR observations

During the commissioning of the VISIR mid-infrared imager/spectrograph at the ESO VLT (UT3, Melipal), the Galactic Center was observed on May 7th – 11th 2004. Many narrowband filters spanning the whole *N*-band (8-13  $\mu\text{m}$ ), as well as the 18.7  $\mu\text{m}$  and 19.5  $\mu\text{m}$  ( $\Delta\lambda = 0.88$  and 0.40  $\mu\text{m}$ ) filters in the *Q*-band were used. In this paper we concentrate on

the 8.6, 11.3, and 12.8  $\mu\text{m}$  ( $\Delta\lambda = 0.42, 0.59,$  and  $0.21 \mu\text{m}$ ) filters in the  $N$ -band, since the highest number of images (and thus the longest integration times) were produced with these filters. The images cover a field of view of approximately  $32'' \times 32''$  at a pixel scale of  $0.127''$  per pixel (see e.g. Lagage et al. 2003 for further details on VISIR). The resulting angular resolution (due to seeing and the diffraction limit) varies between  $0.3''$  at  $8.6 \mu\text{m}$  and approximately  $0.6''$  in the  $Q$ -band. Each of the images supplied by the VISIR pipeline consists of the average of (typically) seven chopped (chopper frequency  $0.25 \text{ Hz}$ , amplitude  $12.5''$ , position angle  $0^\circ$ ) and flat-fielded exposures, with a typical integration time of  $14 \text{ s}$  per averaged image.<sup>1</sup>

### 2.1.1. Additional data

For comparison with shorter wavelengths,  $H$ -,  $K_s$ -,  $L$ - and  $M$ -band ( $1.6, 2.1, 3.8$  and  $4.7 \mu\text{m}$ ) data were taken from Viehmann et al. (2005).

## 2.2. Data reduction

The chopped and flat-fielded exposures supplied by the pipeline were selected based on image quality (FWHM and signal-to-noise ratio) and coadded, resulting in total integration times of  $168, 182, 140, 70$  and  $140$  seconds at  $8.6, 11.3, 12.8, 18.7$  and  $19.5 \mu\text{m}$ , respectively. The final  $19.5 \mu\text{m}$  image is shown in Fig. 1, while a three-color composite of the  $N$ -band images is shown in Fig. 2.

### 2.2.1. Photometry

Flux densities for the MIR sources were obtained using aperture photometry with an aperture of approximately  $1''$ . Additional flux densities were obtained with apertures of  $2''$  and  $0.5''$  in order to correct for confusion effects for closely separated sources, and to optimise the background subtraction. For the purpose of background subtraction, the sky contribution is fitted to an annulus situated between radii of  $1.6''$  and  $2.1''$  (from the center of the aperture) in the case of the  $1''$  aperture, and between  $2.6''$  and  $3.1''$  or between  $1''$  and  $1.5''$  for the  $2''$  and  $0.5''$  apertures, respectively.

---

<sup>1</sup>It should be noted that the unfortunate choice of position angle for chopping results in a negative artifact in the images, since the bright source IRS 8 lies in the corresponding field of view.

Since no suitable calibration stars were observed, the flux density calibration proved difficult. Very few  $N$ - or  $Q$ -band magnitudes or flux densities of Galactic Center sources have been published at present. We used IRS 21 as calibration source, since it is the  $N$ -band source studied in greatest detail (e.g. Gezari et al. 1985; Tanner et al. 2002). We used the flux densities for IRS 21 at 8.8, 12.5, 20.8, and 24.5  $\mu\text{m}$  given by Tanner et al. (2002), assuming that the emission from IRS 21 follows the general shape of the integrated Galactic Center spectrum as measured by ISO (Lutz et al. 1996). For 8.6  $\mu\text{m}$ , we also took into account the flux density at 8.7  $\mu\text{m}$  published by Stolovy et al. (1996). Corrections for the different aperture sizes and background subtraction were applied. For extinction correction, we assumed  $A_V=25$  (Scoville et al. 2003; Viehmann et al. 2005), adopting the extinction law of Moneti et al. (2001) for the  $N$ - and  $Q$ -bands.

We estimate the total uncertainty (i.e. statistical and systematic) of the photometry results as  $\pm 30\%$ , rising to  $\pm 50\%$  for the faintest sources ( $\lesssim 0.5$  Jy). The dominating uncertainty here is that of the flux density calibration, and also the correct background subtraction for the faint sources.

### 3. Results

#### 3.1. New detections

We have obtained photometry for a total of 35 sources at 19.5  $\mu\text{m}$  rising to 64 sources at 8.6  $\mu\text{m}$ . This is probably the largest number of Galactic Center sources investigated in the  $N$ - and  $Q$ -bands up to now and includes the first detection of the Galactic Center Helium-emission-line stars IRS 16NE, IRS 16NW and AF/AHH, as well as the red giants IRS 12N, IRS 14NE and IRS 14SW in the  $N$ -band, as shown in Fig. 3. Additionally, it is now possible to separate the WC9 star IRS 6E (Blum et al. 1996) from the bright extended emission associated with IRS 6W. The corresponding data can be found in table 1.

#### 3.2. SEDs

Combining the VISIR data with shorter wavelength data enables us to construct an unprecedented (for the Galactic Center) number of spectral energy distributions (SEDs) across the whole 1.6 to 19.5  $\mu\text{m}$  range. These are shown in Fig. 4.

### 3.2.1. Classification by SED?

Preliminary analysis of a few typical cases indicates that these SEDs can provide interesting information on the source characteristics, since different source types have SEDs of considerably different shape. This could possibly allow for preliminary classification of presently unclassified sources. The different types of SED found in our sample are as follows:

#### I. Northern Arm embedded sources

These are luminous sources that are embedded in the “Northern Arm” stream of gas and dust, and also in the bar area of the minispiral. IRS 1W, 2L, 5, 10W and 21 belong to this group, which shows very red and fairly featureless SEDs, with their maximum in the  $N$ -band, indicating fairly low temperatures (approximately 300 K according to Gezari et al. 1985). These objects are successfully described as bow shock sources (Tanner et al. 2002, 2003, 2005; Rigaut et al. 2003; Eckart et al. 2004; Geballe et al. 2004). IRS 13E, which is situated in the bar area of the minispiral, shows similar characteristics, although it is clearly hotter (Gezari et al. 1996), with the embedded source identified as a cluster of massive young stars (e.g. Krabbe et al. 1995; Najarro et al. 1997; Eckart et al. 2004; Maillard et al. 2004).

#### II. Lower luminosity bow shock sources

These sources are less luminous and often situated close to the edge of the minispiral. In almost all cases, they are identified as bow-shock sources by their morphology, the bow-shock structure being visible in high-resolution  $L$ - or  $M$ -band images obtained with adaptive optics (see e.g. Genzel et al. 2003; Clénet et al. 2004b, for such images). A striking example (source 41 in our sample) is presented by Clénet et al. (2004a). These sources show very red SEDs with their maxima longwards of  $12\ \mu\text{m}$ . Their characteristics at shorter wavelengths are diverse: some show a fairly flat SED between  $1.6$  and  $11.3\ \mu\text{m}$ , while others exhibit a minimum around  $8.6\ \mu\text{m}$ . These differences are probably due to differences between the type of stars powering the bow-shocks (see below), and due to the presence and density of the dusty medium that surrounds them and with which they interact. We propose that IRS 2S, which has been classified as a cool red giant by Blum et al. (1996), belongs to this type of source, since it shows a flat SED from  $1.6$  to  $11.3\ \mu\text{m}$  and brightens considerably at longer wavelengths.

#### III. Cool stars

The SEDs of these sources all have their maximum in the  $2$  to  $5\ \mu\text{m}$  region. The SEDs then fall off to the  $N$ -band, where they appear to flatten out. In those cases which are still detectable at wavelengths longer than  $8.6\ \mu\text{m}$  (despite decreasing resolution and sensitivity),

the  $N$ - and  $Q$ -band flux densities of this type of source appear to be more or less constant for each source. This effect is probably due to circumstellar dust emission, which is to be expected, since the brightest cool red giants at the Galactic Center have been identified as AGB stars (Ott et al. 1999; Clénet et al. 2001) and are thus situated in a mass-loss phase, creating dust envelopes. A *very* weak bow-shock type interaction with the surrounding medium is also possible in the case of AGB stars, since they have fairly strong stellar winds.

#### IV. Hot stars

These sources exhibit SEDs that fall off steeply (steeper than those of cool stars) between 5 and 8  $\mu\text{m}$ . Therefore, the  $M - N$  color (more particularly  $M - m_{8.6\mu\text{m}}$ ) appears to be a criterion for distinguishing hot and cool stars, if spectroscopic information is not available. The clearly identified hot stars in our sample fall into two distinctive subgroups: The Galactic Center He-stars IRS 16NE, IRS 16NW and AF/AHH, which are frequently classified as LBV or Ofpe/WN9 (e.g. Clénet et al. 2001), are brightest at short wavelengths with SEDs that fall monotonically towards longer wavelengths. The dominant source of infrared emission is thus probably photospheric, with a wind (or faint bow shock) contribution in the  $L$ - and  $M$ -band (see Viehmann et al. 2005). On the other hand, IRS 29 and IRS 6E, which have been classified as WC9 Wolf-Rayet stars (e.g. Blum et al. 1996), exhibit SEDs which peak in the  $L$ - and  $M$ -bands, while their  $H$ - and  $K$ -band flux densities appear to be considerably lower. The corresponding interpretation is that these stars are surrounded by a self-generated dust shell which partly extincts the shorter wavelength emission and itself emits strongly at 3-5  $\mu\text{m}$  (see also Moultaika et al. 2004).

#### V. IRS 3

This source clearly stands apart from all other Galactic Center mid-infrared sources. While Horrobin et al. (2004) classified IRS 3 as a WC5/6 star, Pott et al. (2005) and R. Genzel (private communication) have pointed out that this identification probably applies to a different, fainter source situated approximately 0.12'' to the east of IRS 3. This does not rule out that IRS 3 may be a massive Wolf-Rayet star, but Pott et al. (2005) have also shown that it may be an extreme AGB star. The true nature of IRS 3 therefore remains unclear. Among the bright  $N$ -band sources, it is the most compact (see new interferometric MIDI VLTI results by Pott et al. 2005), apart from IRS 7 (Gezari et al. 1985). It is also the brightest source in the  $M$ -band and one of the brightest over the whole mid-infrared region covered here ( $L$ - to  $Q$ -band), while it appears unremarkable in the  $K$ -band and very faint at shorter wavelengths. The shape of the SED of IRS 3 is thus unlike any of the typical cases discussed at present: IRS 3 is much fainter than the luminous bow-shock sources in the near-infrared, while clearly hotter (approximately 400 to 600 K, see Gezari et al. 1985,

1996) and thus showing maximum emission at a shorter wavelength ( $M$ -band vs.  $10\ \mu\text{m}$ ). Compared to luminous cool stars (IRS 7, IRS 10E\*), IRS 3 is clearly fainter at near-infrared wavelengths and much brighter in the  $N$ - and  $Q$ -bands. The same applies to the comparison of IRS 3 with the hot stars in our sample. However, a certain similarity to the SED of IRS 29 (WC9 type) is discernible: The source is faint and obviously extinguished in the  $H$ -band, has a maximum at short midinfrared wavelengths ( $L$ - and  $M$ -band) and shows a fairly clear absorption feature at approximately  $10\ \mu\text{m}$  (see section 3.2.2). The reason for this similarity is that the emission from both objects comes from thick, self-generated dust shells (compare Viehmann et al. 2005).

### 3.2.2. Silicate dust

The spectrum between  $8.6\ \mu\text{m}$  and  $12\ \mu\text{m}$  is especially interesting, since there is a broad interstellar silicate absorption feature at  $9.7\ \mu\text{m}$  (Lutz et al. 1996). Our data at  $11.3\ \mu\text{m}$  lie on the flank of this absorption; consequently, sources that are underluminous at this wavelength appear to show additional, and therefore *intrinsic* silicate absorption, i.e. absorption in excess of that found in the overall ISO spectrum (Lutz et al. 1996). IRS 3 and IRS 6W clearly show this effect, which is also visible in Fig. 2 (lack of green), as do IRS 34 (both components) and source 24. The most likely explanation is that these stars are surrounded by (possibly self-generated) dust shells containing additional silicate dust. The cool star IRS 10E\* and the hot stars IRS 6E and IRS 29, which have been identified as WC9 Wolf-Rayet stars (e.g. Blum et al. 1996), might also show signs of such absorption, although the steepening of their SED is slight and may therefore be insignificant. In the case of the WC9 stars, intrinsic silicate absorption is difficult to explain, however, one possibility is that the absorption is due to collected material not originally produced by the stars themselves. Enhanced, patchy foreground extinction over the whole IRS 3 to IRS 6W area is a possible alternative explanation.

In contrast, none of the luminous, bow-shock dominated sources shows intrinsic silicate absorption. Therefore they appear yellow in the color image shown in Fig. 2. It seems that the lower luminosity bow-shock sources also do not show such an absorption effect.

### 3.2.3. Excess emission at $12.8\ \mu\text{m}$

Due to the shape of the Galactic Center spectrum (e.g. Lutz et al. 1996), slightly higher flux densities are to be expected at  $12.8\ \mu\text{m}$ . This is clearly visible in the SEDs obtained

from our observations, however, some sources show a larger excess, which appears to indicate additional intrinsic emission at  $12.8 \mu\text{m}$  and must be explained.

While Willner (1978) state that the  $12.8 \mu\text{m}$  Ne II line emission at the Galactic Center is extended and not associated with compact mid-infrared sources, Lacy et al. (1979, 1980) find that part of the Ne II emission comes from compact regions of ionized gas which are indeed associated with mid-infrared continuum sources. Consequently, Ne II line emission is a possible explanation for at least some of these excesses.

In the case of IRS 10E\* (and IRS 9 if the small excess of this source is significant), we attribute the  $12.8 \mu\text{m}$  excess to a narrow streamer of enhanced emission running approximately southwards from IRS 5, which probably resulted in an insufficient background subtraction (see section 2.2.1). The excess  $12.8\mu\text{m}$  emission of IRS 2, 6W and 13 could also be the result of insufficient background subtraction due to the clumpy nature of the extended emission from this part of the minispiral, which shows quite a complex structure.

The excess  $12.8 \mu\text{m}$  emission clearly visible in the SEDs of IRS 3, 7 and possibly 29 (also visible in Fig. 2), however, cannot be explained in this fashion. Since Lacy et al. (1980) state that IRS 3 and IRS 7 do not have associated gas clouds, it appears unlikely that the excess of these sources is due to Ne II line emission. We therefore suggest that the excess of these sources at  $12.8 \mu\text{m}$  is due to continuum emission caused by a faint bowshock-like interaction of the stellar winds of these stars with the surrounding medium. Since this is a small effect, the corresponding excess that is to be expected at  $11.3 \mu\text{m}$  could be masked by intrinsic silicate absorption (see above). The absence of a clear excess at  $18.7 \mu\text{m}$  in these sources does not rule out such an explanation, since the known bow-shock sources (types I. and II. in section 3.2.1) show diverse characteristics in the  $Q$ -band (the fainter sources have their maxima there, the brighter ones have their maxima in the  $N$ -band).

### 3.3. Unusual sources east of IRS 5

Among the most intriguing mid-infrared sources at the Galactic Center are four bright pointlike sources located to the east of the bright Northern Arm source IRS 5. The nature of these sources, which we refer to as IRS 5NE, IRS 5E, IRS 5S, and IRS 5SE (see Fig. 3), is currently unclear. They are remarkable in that they are almost as bright as IRS 7 in the  $N$ -band, while they appear much less prominent at shorter wavelengths, although they remain bright in the  $L$ - and  $M$ -bands. Detailed inspection reveals that IRS 5SE, which appears *slightly* extended at longer wavelengths, is in fact double, consisting of a blue point source to the east (IRS 5SE2, dominant component in  $K$ -band images) and a fainter source

to the west, which shows a tail like structure and is the main source of emission at longer wavelengths (IRS 5SE1, dominant component in  $N$ - and  $Q$ -band). This may represent an intriguing case of possible interaction, either of the two sources with each other – if they lie close together along the line of sight – or of the western component with the surrounding medium. A further possibility is that a bow shock generated by the eastern component is superimposed on the western one, however, their separation makes this unlikely.

All of these sources except IRS 5SE2 show SEDs that are either flat between 3.8 and 20  $\mu\text{m}$  (IRS 5NE) or increase dramatically towards longer wavelengths. Therefore, these sources show similar characteristics to identified lower-luminosity bow-shock sources (e.g. IRS 9N, see section 3.2.1), however, their appearance on high-resolution NAOS/CONICA images does not indicate such a structure, which is normally visible for this type of source (IRS 5SE1 is the obvious exception here). It therefore appears that a reliable classification and/or understanding of these sources can only be achieved with spectroscopic methods or possibly interferometry using VLTI.

#### 4. Conclusion

We have presented mid-infrared photometry of the Galactic Center from images obtained with the VISIR camera at the ESO VLT. In combination with shorter wavelength data (Viehmann et al. 2005), we were able to construct SEDs for an unprecedented number of sources (for the Galactic Center) in this wavelength regime. We find that different source types show characteristic differences in the shape of their SEDs, which should help in the preliminary classification of compact mid-infrared sources. In particular, we find that additional, i.e. intrinsic, absorption at approximately 10  $\mu\text{m}$  is a sign of dust formation. Many of the brightest Galactic Center mid-infrared sources, however, appear to be bow-shock powered and do not show dust formation features in their SEDs. In addition, we find that hot and cool stars show different  $M - m_{8.6\mu\text{m}}$  colors, with the cool stars showing redder colors, as is to be expected.

We have reported on four fairly bright  $N$ -band point sources located to the east of the bright Northern Arm source IRS 5. The most likely explanation for their unusual appearance at mid-infrared wavelengths is that these sources are bow-shock sources of lower luminosity than the typical Northern Arm sources.

The main uncertainty in our results is due to calibration uncertainties as a result of the lack of suitable reference observations. Therefore, mid-infrared observations of the Galactic Center remain necessary in order to obtain more complete information on the dusty mid-

infrared sources in this intriguing environment.

This work was supported in part by the Deutsche Forschungsgemeinschaft (DFG) via grant SFB 494.

## REFERENCES

- Becklin, E. E., Matthews, K., Neugebauer, G., & Willner, S. P. 1978, *ApJ*, 219, 121
- Becklin, E. E., & Neugebauer, G. 1968, *ApJ*, 151, 145
- . 1969, *ApJ*, 157, L31+
- Blum, R. D., Sellgren, K., & Depoy, D. L. 1996, *ApJ*, 470, 864
- Clénet, Y., Rouan, D., Gendron, E., Lacombe, F., Lagrange, A.-M., Mouillet, D., Magnard, Y., Rousset, G., Fusco, T., Montri, J., Genzel, R., Schödel, R., Ott, T., Eckart, A., Marco, O., & Tacconi-Garman, L. 2004a, *A&A*, 417, L15
- Clénet, Y., Rouan, D., Gendron, E., Montri, J., Rigaut, F., Léna, P., & Lacombe, F. 2001, *A&A*, 376, 124
- Clénet, Y., Rouan, D., Gratadour, D., Lacombe, F., Gendron, E., Genzel, R., Ott, T., Schödel, R., & Léna, P. 2004b, *A&A*, 424, L21
- Eckart, A., Moultaqa, J., Viehmann, T., Straubmeier, C., & Mouawad, N. 2004, *ApJ*, 602, 760
- Geballe, T. R., Rigaut, F., Roy, J.-R., & Draine, B. T. 2004, *ApJ*, 602, 770
- Genzel, R., Schödel, R., Ott, T., Eisenhauer, F., Hofmann, R., Lehnert, M., Eckart, A., Alexander, T., Sternberg, A., Lenzen, R., Clénet, Y., Lacombe, F., Rouan, D., Renzini, A., & Tacconi-Garman, L. E. 2003, *ApJ*, 594, 812
- Gezari, D., Dwek, E., & Varosi, F. 1996, in *IAU Symp. 169: Unsolved Problems of the Milky Way*, 231–+
- Gezari, D. Y., Shu, P., Lamb, G., Tresch-Fienberg, R., Fazio, G. G., Hoffmann, W. F., Gatley, I., & McCreight, C. 1985, *ApJ*, 299, 1007

- Horrobin, M., Eisenhauer, F., Tecza, M., Thatte, N., Genzel, R., Abuter, R., Iserlohe, C., Schreiber, J., Schegerer, A., Lutz, D., Ott, T., & Schödel, R. 2004, *Astronomische Nachrichten*, 325, 88
- Krabbe, A., Genzel, R., Eckart, A., Najarro, F., Lutz, D., Cameron, M., Kroker, H., Tacconi-Garman, L. E., Thatte, N., Weitzel, L., Drapatz, S., Geballe, T., Sternberg, A., & Kudritzki, R. 1995, *ApJ*, 447, L95+
- Lacy, J. H., Baas, F., Townes, C. H., & Geballe, T. R. 1979, *ApJ*, 227, L17
- Lacy, J. H., Townes, C. H., Geballe, T. R., & Hollenbach, D. J. 1980, *ApJ*, 241, 132
- Lagage, P.-O., Pel, J.-W., Claret, A., Damstra, S., Dubreuil, D., Durand, G. A., Elswijk, E., Galdemard, P., de Jong, A. N., Kroes, G., Lyraud, C., Pantin, E., Pragt, J., Rio, Y., Schoenmaker, A., Authier, M., Belorgey, J., Gournay, J.-F., Lortholary, M., Lussignol, Y., & Veyssiere, C. 2003, in *Instrument Design and Performance for Optical/Infrared Ground-based Telescopes*. Edited by Iye, Masanori; Moorwood, Alan F. M. *Proceedings of the SPIE*, Volume 4841, pp. 923-931 (2003)., 923–931
- Low, F. J., Kleinmann, D. E., Forbes, F. F., & Aumann, H. H. 1969, *ApJ*, 157, L97+
- Lutz, D., Feuchtgruber, H., Genzel, R., Kunze, D., Rigopoulou, D., Spoon, H. W. W., Wright, C. M., Egami, E., Katterloher, R., Sturm, E., Wieprecht, E., Sternberg, A., Moorwood, A. F. M., & de Graauw, T. 1996, *A&A*, 315, L269
- Maillard, J. P., Paumard, T., Stolovy, S. R., & Rigaut, F. 2004, *A&A*, 423, 155
- Moneti, A., Stolovy, S., Blommaert, J. A. D. L., Figer, D. F., & Najarro, F. 2001, *A&A*, 366, 106
- Moultaka, J., Eckart, A., Viehmann, T., Mouawad, N., Straubmeier, C., Ott, T., & Schödel, R. 2004, *A&A*, 425, 529
- Najarro, F., Krabbe, A., Genzel, R., Lutz, D., Kudritzki, R. P., & Hillier, D. J. 1997, *A&A*, 325, 700
- Ott, T., Eckart, A., & Genzel, R. 1999, *ApJ*, 523, 248
- Pott, J.-U., Eckart, A., Glindemann, A., Viehmann, T., Schoedel, R., Straubmeier, C., Leinert, C., Feldt, M., Genzel, R., & Robberto, M. 2005, *The Messenger*, 119, 43
- Reid, M. J., Menten, K. M., Genzel, R., Ott, T., Schödel, R., & Eckart, A. 2003, *ApJ*, 587, 208

- Reid, M. J., Readhead, A. C. S., Vermeulen, R. C., & Treuhaft, R. N. 1999, *ApJ*, 524, 816
- Rigaut, F., Geballe, T. R., Roy, J.-R., & Draine, B. T. 2003, *Astronomische Nachrichten Supplement*, 324, 551
- Scoville, N. Z., Stolovy, S. R., Rieke, M., Christopher, M., & Yusef-Zadeh, F. 2003, *ApJ*, 594, 294
- Stolovy, S. R., Hayward, T. L., & Herter, T. 1996, *ApJ*, 470, L45+
- Tanner, A., Ghez, A. M., Morris, M., Becklin, E. E., Cotera, A., Ressler, M., Werner, M., & Wizinowich, P. 2002, *ApJ*, 575, 860
- Tanner, A., Ghez, A. M., Morris, M. R., & Christou, J. C. 2005, *ApJ*, 624, 742
- Tanner, A. M., Ghez, A. M., Morris, M., & Becklin, E. E. 2003, *Astronomische Nachrichten Supplement*, 324, 597
- Viehmann, T., Eckart, A., Schödel, R., Moutaka, J., Straubmeier, C., & Pott, J.-U. 2005, *A&A*, 433, 117
- Willner, S. P. 1978, *ApJ*, 219, 870

Table 1. Extinction corrected flux densities of compact  $N$ -band sources.

ID	Name	$\Delta\alpha(^{\prime\prime})^a$	$\Delta\delta(^{\prime\prime})^a$	Flux density (Jy) <sup>b</sup>								
				Wavelength ( $\mu\text{m}$ )	...	...	1.6	2.1	3.8	4.7	8.6	11.3
1	IRS 1W	5.1	-5.05	1.37	2.29	12.65	16.29	20.42	16.35	22.93	16.48	18.94
2	...	5.8	-5.3	...	...	...	...	2.21	1.2	3.1	...	...
3 <sup>c</sup>	...	3.5	-4.0	0.1	0.12	0.25	0.31	0.13	0.42	0.6	0.98	0.46
4	...	3.5	-4.05	...	...	...	...	0.24	...	...	...	...
5	...	5.3	-6.55	...	0.07	0.12	0.15	0.06	0.03	0.13	...	...
6	IRS 2L	-3.6	-9.45	0.13	0.48	2.98	3.98	5.26	4.72	7.49	2.05	2.58
7	IRS 2S <sup>c</sup>	-4.0	-11.05	0.5	0.49	0.8	0.64	0.68	0.61	1.3	0.75	1.01
8	IRS 3	-2.45	-1.8	0.07	0.46	13.61	30.2	13.42	6.57	12.85	5.85	6.88
9	...	-2.25	-3.3	...	...	...	...	0.21	0.03	0.31	...	...
10	...	-1.0	-1.65	...	...	...	...	0.14	0.06	0.14	0.23	...
11	IRS 4	10.3	-11.5	...	...	...	...	0.11	0.19	0.45	0.48	0.61
12	...	9.8	-14.4	...	...	...	...	0.14	0.27	0.63	0.77	0.76
13	IRS 5	8.5	4.15	...	...	4.27	4.88	5.11	4.21	5.85	3.21	2.85
14	IRS 5NE	12.7	5.0	...	...	0.53	0.8	0.51	0.6	0.56	0.95	0.74
15	IRS 5E	10.8	3.7	...	...	0.15	0.21	0.59	1.06	1.54	1.58	1.72
16	...	10.0	4.25	...	...	...	...	0.04	...	...	...	...
17	...	11.15	2.9	...	...	...	...	0.05	...	...	...	...
18	IRS 5S	9.0	2.35	...	...	0.36	0.43	0.63	0.51	0.38	0.63	1.06
19	IRS 5SE1	10.55	1.3	...	...	0.19	0.18	0.5	0.97	1.1	2.84	3.58
20	IRS 5SE2	10.95	1.1	...	...	...	...	0.04	0.09	0.13	...	...
21	...	12.8	-0.15	...	...	1.88	1.03	0.08	0.08	0.12	0.21	...
22	IRS 6W	-7.5	-4.25	0.79	0.7	0.87	1.21	3.67	2.95	8.0	2.95	3.37
23	IRS 6E	-5.3	-4.8	0.63	1.22	3.42	3.44	0.21	0.04	0.17	0.16	...
24	...	-7.35	-7.25	0.09	0.1	0.21	0.28	0.19	0.08	0.58	0.43	0.43
25	IRS 7	0.0	0.0	5.04	2.58	18.97	12.59	1.47	1.14	1.75	0.36	0.41
26	...	-0.25	2.3	...	...	...	...	0.05	0.03	0.11	0.07	0.11
27	IRS 15	1.1	5.65	...	...	1.71	1.28	0.14	0.12	0.13	0.08	0.13
28 <sup>c</sup>	...	3.65	1.55	...	0.33	0.32	0.44	0.15	0.24	0.32	0.4	0.34
29	IRS 9	5.4	-11.95	1.31	1.43	2.06	1.15	0.21	0.13	0.21	0.11	0.26
30	IRS 9N <sup>c</sup>	5.4	-11.45	0.24	0.18	0.54	0.65	0.59	0.76	1.21	0.87	1.37
31	...	3.5	-10.9	0.01	...	0.24	...	3.68	2.6	3.58	1.4	2.94
32	...	4.05	-12.9	0.02	0.02	0.27	0.45	2.93	2.77	3.9	2.13	5.51
33	...	5.0	-16.0	0.07	0.06	0.07	...	0.82	0.94	...	...	...
34	...	3.4	-16.9	...	...	...	...	0.03	...	...	...	...
35	IRS 10W	6.35	-0.5	0.45	0.95	3.72	6.49	11.06	10.31	11.85	9.32	9.75
36	IRS 10E*	7.5	-1.45	0.24	1.04	4.9	5.5	0.64	0.25	0.75	0.32	0.37

Table 1—Continued

ID	Name	$\Delta\alpha(^{\prime\prime})^a$	$\Delta\delta(^{\prime\prime})^a$	Flux density (Jy) <sup>b</sup>								
				Wavelength ( $\mu\text{m}$ )	...	...	1.6	2.1	3.8	4.7	8.6	11.3
37	...	6.55	2.05	...	...	...	...	0.1	...	...	...	...
38	...	7.8	-0.4	0.05	0.04	0.05	...	0.21	0.38	...	...	...
39	...	6.2	-8.45	...	...	...	...	0.46	0.56	1.67	0.99	0.71
40	...	6.1	-9.55	...	...	...	...	0.48	0.12	0.76	...	...
41 <sup>c</sup>	...	3.2	-2.2	0.05	0.1	0.15	...	0.01	0.13	...	...	...
42	IRS 12N	-3.5	-12.45	1.37	1.66	2.62	1.77	0.15	0.12	0.1	...	...
43	...	-3.8	-14.9	...	...	...	...	0.02	0.03	...	...	...
44	IRS 13E	-3.35	-7.1	0.92	2.05	3.96	3.37	4.28	4.49	6.16	2.11	2.89
45	IRS 13W	-4.2	-7.6	0.23	0.37	0.76	0.42	0.25	2.02	2.59	1.1	2.0
46 <sup>c</sup>	...	-2.65	-8.0	...	...	...	...	0.36	0.24	0.74	...	...
47	IRS 13N	-3.15	-6.5	0.01	0.03	1.34	1.58	0.38	0.65	1.11	0.55	0.58
48	IRS 13NE	-2.85	-7.0	...	0.04	0.64	0.98	0.43	0.67	1.13	0.47	0.67
49	IRS 14NE	0.7	-13.75	1.24	1.41	0.97	0.47	0.05	0.05	0.08	0.17	...
50	IRS 14SW	-0.4	-14.5	1.25	1.25	0.6	0.25	0.02	0.02	0.02	...	...
51	...	1.1	-12.65	0.17	0.13	0.08	...	0.05	0.06	0.2	0.55	0.52
52	AF/AHH	-6.65	-12.45	0.7	0.56	0.39	0.38	0.02	0.01	...	...	...
53	IRS 20	-2.2	-11.95	0.65	0.49	0.39	0.24	0.02	0.05	0.15	...	...
54	IRS 21	2.15	-8.35	0.17	0.57	3.58	4.29	4.56	4.57	5.44	3.76	4.1
55	IRS 29	-1.75	-4.2	0.15	0.6	2.04	1.98	0.15	0.02	0.04	...	...
56	IRS 33SW	-0.4	-8.7	0.55	0.44	0.42	0.23	0.08	0.05	0.09	...	...
57	IRS 34(SW)	-4.05	-4.0	...	0.01	0.16	0.2	0.12	0.04	0.16	...	...
58	IRS 34NE	-3.65	-3.55	0.13	0.16	0.33	0.31	0.14	0.08	0.18	0.13	0.19
59	IRS 33NW	-0.9	-7.25	0.28	0.27	0.23	0.16	0.69	0.29	0.61	0.68	0.73
60	...	-1.65	-6.15	0.14	0.1	0.12	0.14	1.27	1.32	1.9	1.37	0.66
61	IRS 16NW	-0.1	-4.45	1.47	0.96	0.52	0.36	0.01	...	...	...	...
62	IRS 16NE	2.75	-4.7	3.61	1.77	1.61	1.18	0.08	...	...	...	...
63	...	1.25	-4.65	...	...	...	...	0.01	0.01	0.05	...	...
64	SgrA* Clump	-0.25	-5.65	0.04	0.06	0.07	...	0.02	0.17	0.23	0.32	0.29

<sup>a</sup> Position offsets are relative to IRS 7 ( $17^{\text{h}}45^{\text{m}}40^{\text{s}}.052$ ,  $-29^{\circ}00'33''.659$ , see Reid et al. 1999, 2003) and are accurate to  $\pm 0.15''$ .

<sup>b</sup> Photometry is accurate to  $\pm 30\%$ , or  $\pm 50\%$  for sources fainter than  $\sim 0.5$  Jy. The corresponding aperture size is approximately  $1''$ .

<sup>c</sup> Lower luminosity bow-shock source, see section 3.2.1.

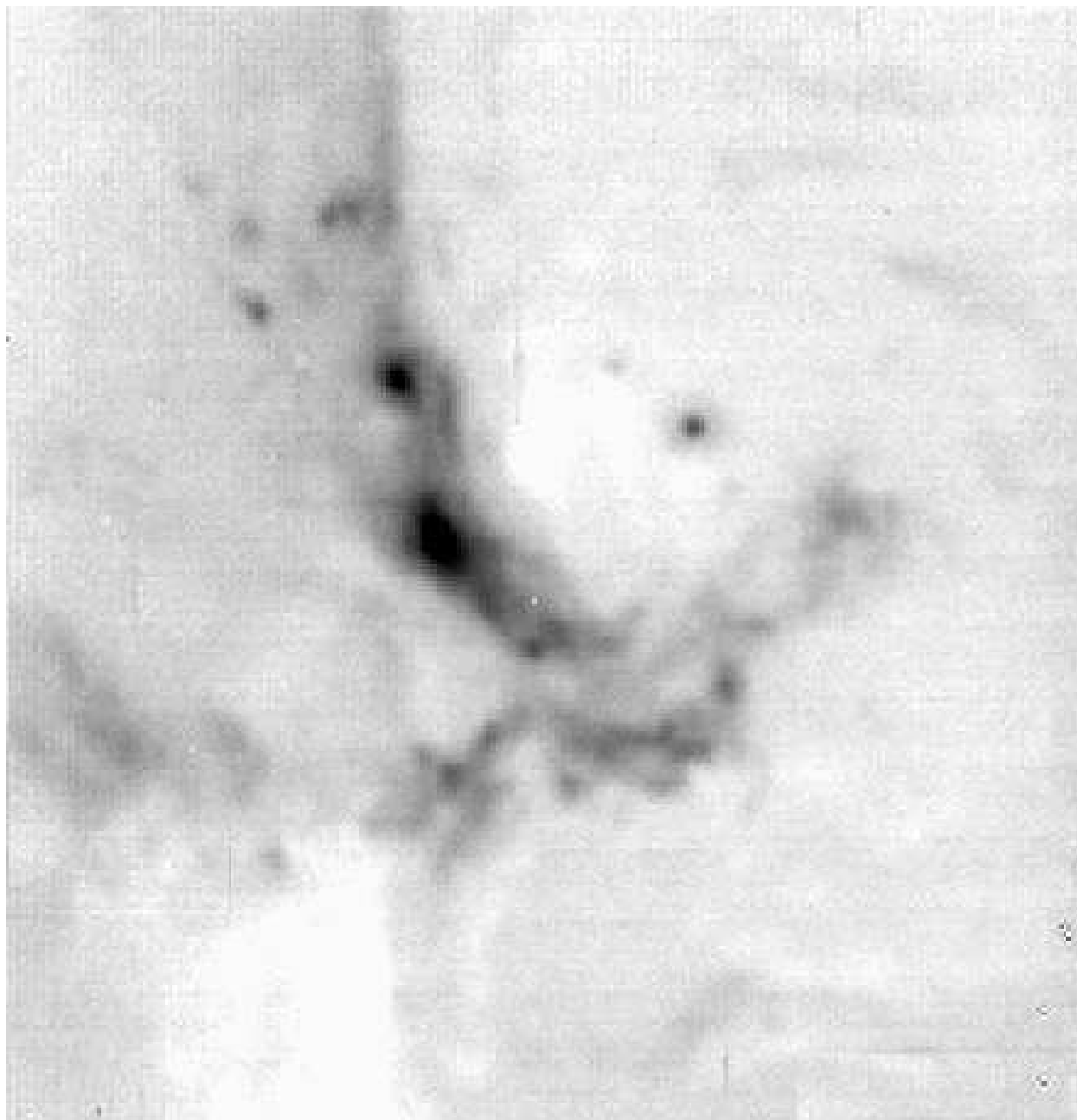


Fig. 1.— VISIR  $19.5 \mu\text{m}$  image of the Galactic Center. The field of view is  $32'' \times 32''$ . East is to the left, and north is up.

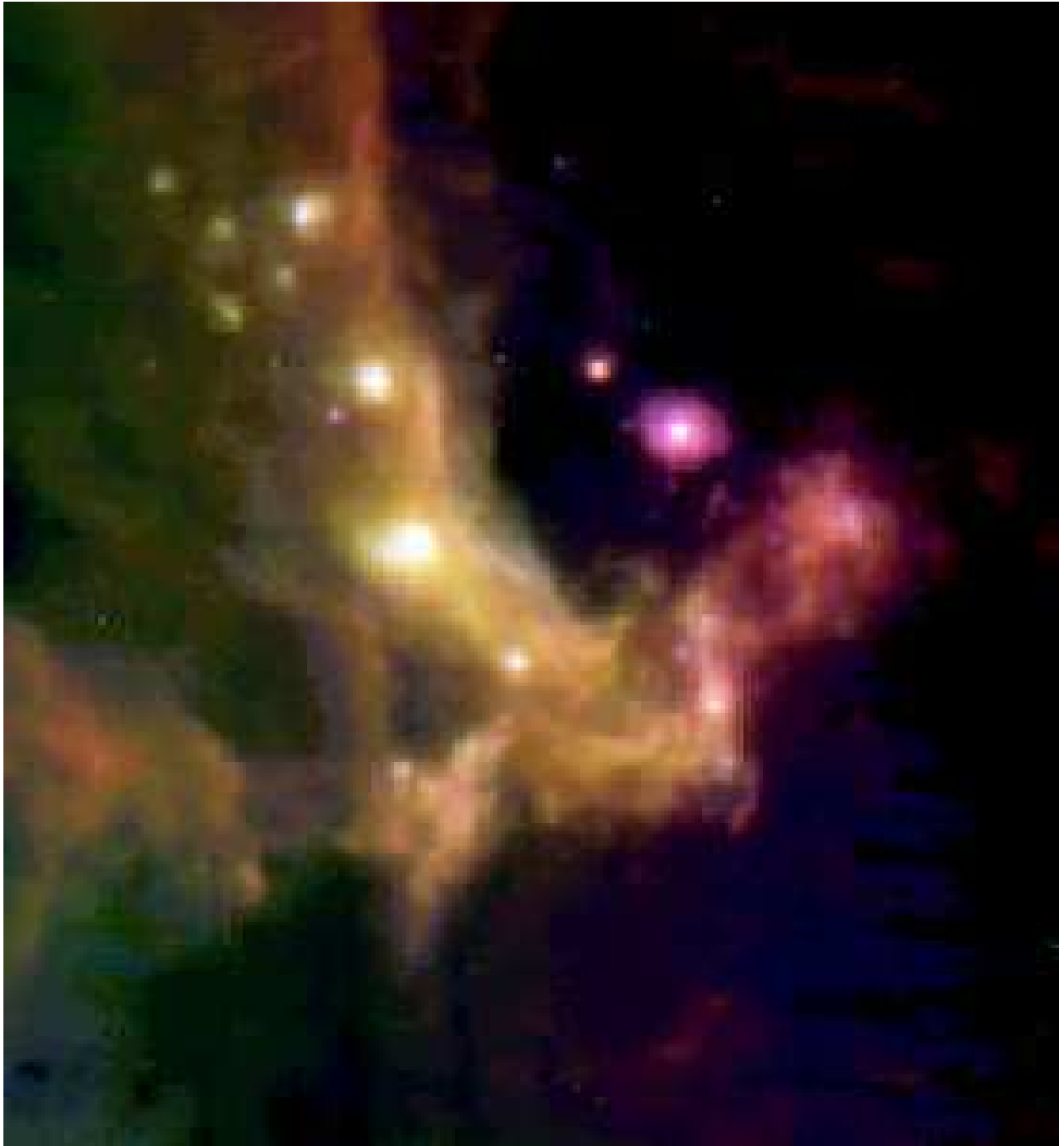


Fig. 2.— VISIR *N*-band three-color composite view of the Galactic Center. The blue channel is  $8.6 \mu\text{m}$ , green is  $11.3 \mu\text{m}$  and red is  $12.8 \mu\text{m}$ .

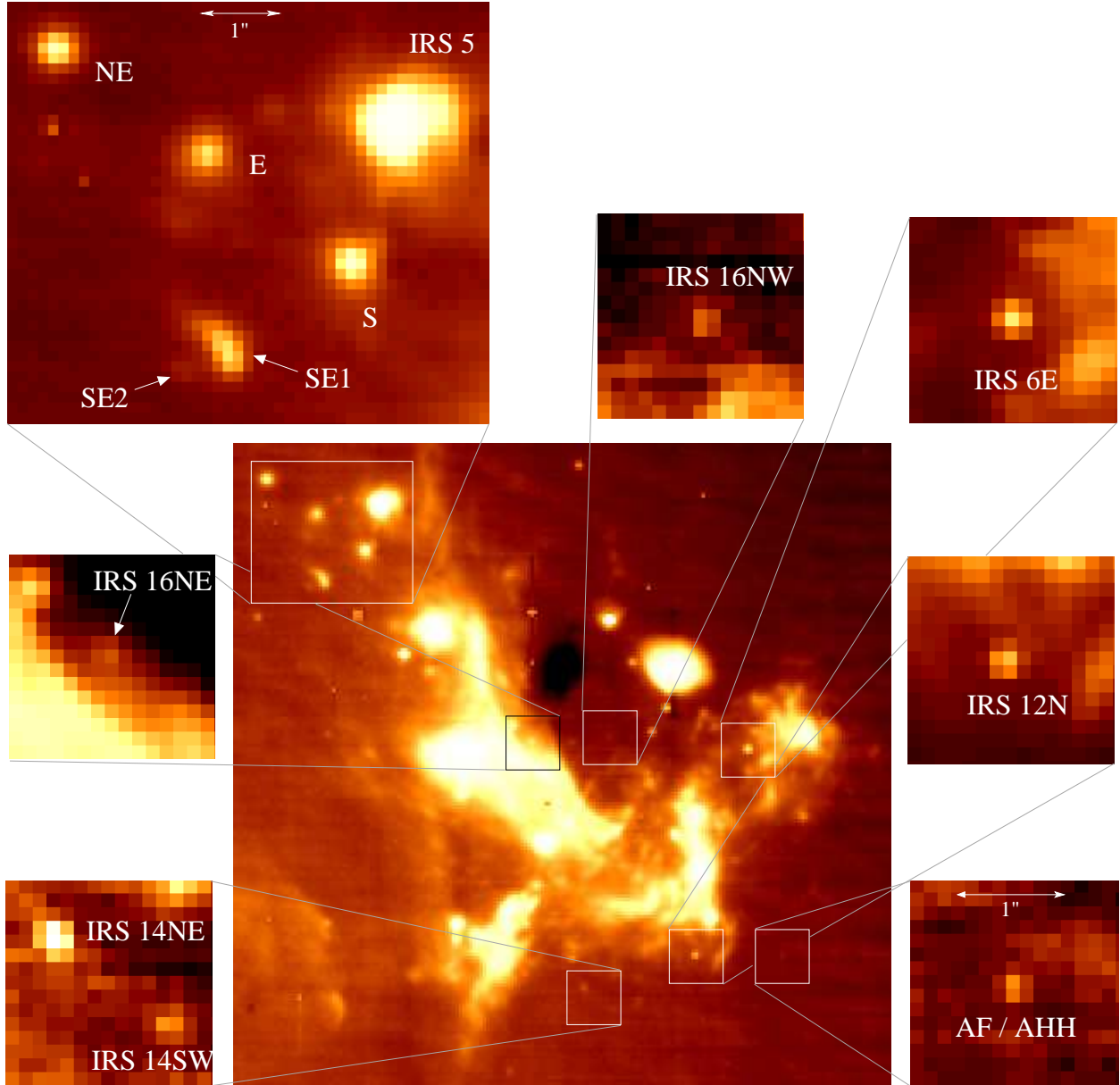


Fig. 3.— VISIR 8.6  $\mu\text{m}$  view of the Galactic Center. The field of view is approximately  $24'' \times 24''$ . The insets show enlarged views of the newly detected stars AF/AHH, IRS 6E, IRS 12N, IRS 14NE, IRS 14SW, IRS 16NE and IRS 16NW (see section 3.1), as well as the intriguing group of bright sources located to the east of IRS 5 (upper left, see section 3.3).

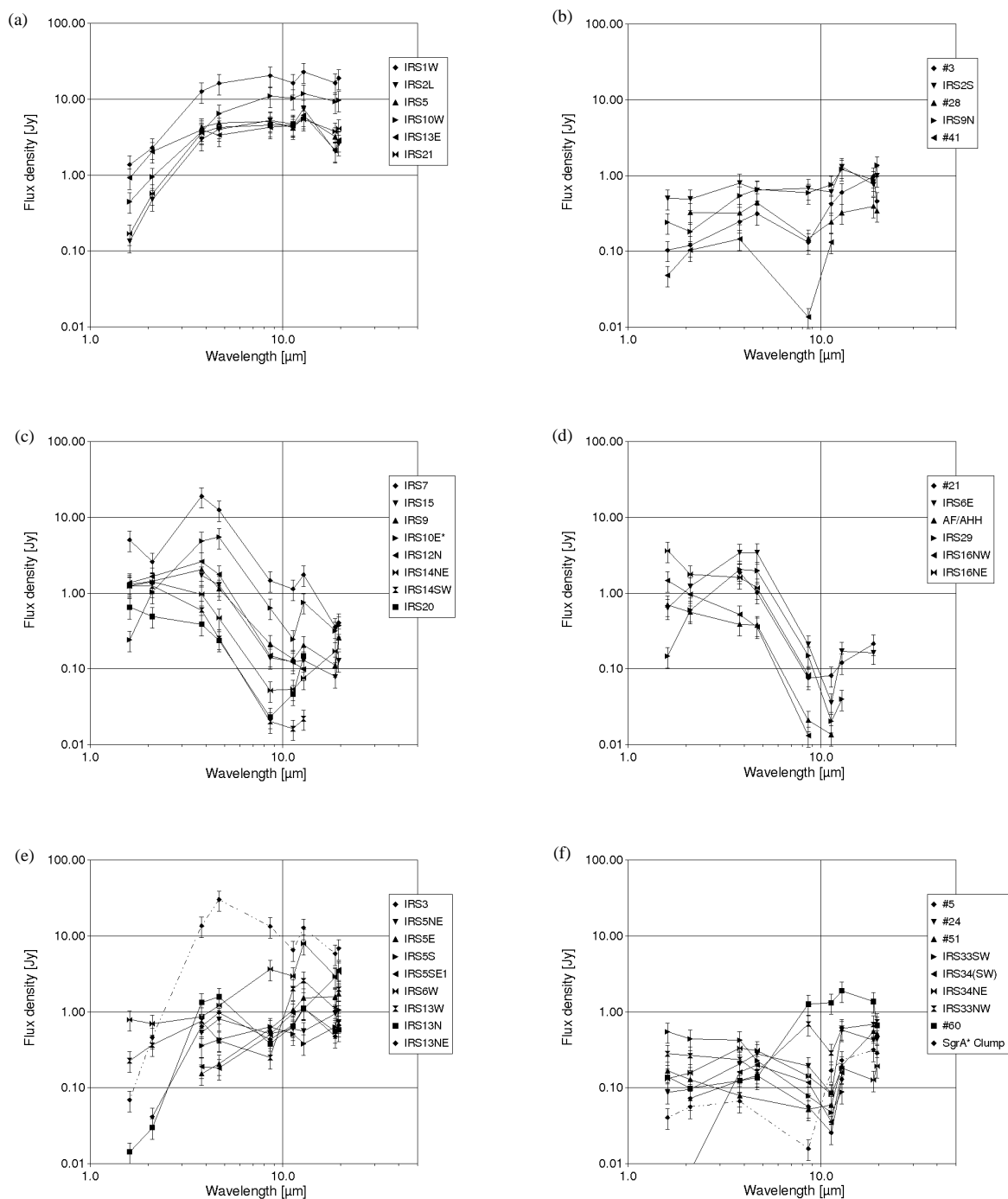


Fig. 4.— Spectral energy distributions of Galactic Center mid-infrared sources. The SEDs have been grouped by type, as described in section 3.2.1: (a) shows the typical luminous bow-shock sources, (b) shows lower luminosity bow-shock sources, (c) cool stars, (d) hot stars, while (e) and (f) show the SEDs of unclassified sources. In (e) and (f), IRS 3 and the Sgr A\* clump are distinguished by a dash-dotted line.